AGU PUBLICATIONS

Geophysical Research Letters

Supporting Information for

Pore space topology controls ultrasonic waveforms in dry volcanic rocks.

Maria Del Pilar Di Martino[1,2], Luca De Siena[3], and Nicola Tisato[4]

[1] School of Geosciences, University of Aberdeen, Aberdeen, UK.

[2] WASM: Mineral, Energy and Chemical Engineering, Curtin University, Perth, Australia.

[3] Institute of Geosciences, Johannes Gutenberg University Mainz, Mainz, Germany.

[4]Jackson School of Geosciences, The University of Texas at Austin, Austin, TX, USA.

Contents of this file

This file contains supplementary information separated into nine (9) sections

SM-1. Parameters for modelling in SPECFEM2D

Input Parameter	**Synthetic rocks**	**R1H**
Simulation	Forward	Forward
Partitioning method	Scotch	Scotch
Control nodes per element	4	9
Number of steps NSTEP	100,000	800,000
Time step DT	4.0 e-09 s	0.38 e-09 s
Time Stepping	Newmark (2^{nd})	Newmark (2^{nd})
Wave Type	SH	SH
*Boundary Conditions	Stacey, absorbing boundary	Stacey, absorbing boundary
Models	2	2
Model 1 (rock matrix)	ρ= 2940 kg/cc Vp= 2860 m/s Vs= 1490 m/s	ρ= 2940 kg/cc Vp= 2860 m/s Vs= 1490 m/s
**Model 2 (pores)	ρ= 1.020 kg/cc Vp= 330 m/s Vs= 0 m/s	ρ= 1.020 kg/cc Vp= 330 m/s Vs= 0 m/s
Source	Ricker	Ricker
Dominant Source Frequency	100 kHz	100 kHz
Source Amplification Factor	1.0d10	1.0d10
Receiver seismo-type	Displacement	Displacement

*Note that PML boundary conditions are not implemented in SPECFEM2D for SH propagation.

** In the paper the simulations are performed for SH waves (antiplane shear), therefore these parameters are not used in the governing equations and only specified here because SPECFEM2D requires to input then.

- Mesh Generation using GMSH (http://gmsh.info/)

Setting up mesh	**Synthetic**	**R1H**
Total Number of Elements	8,945	136,854
Total number of nodes	8,794	164,534
Number of grid points in the mesh	141,617	2,026,108
Absorbing boundaries	Top, left, bottom, right	Top, left, bottom, right
Free Boundaries	none	none
Elements in contact with absorbing surface	304	1504
Xmin / Xmax	0.0 / 2.5e-2	0.0 / 2.5e-2
Zmin / Zmax	0.0 / 5.0e-5	0.0 / 5.0e-5
Max grid size	9.618 e-4	2.129 e-4
Min grid size	1.129 e-4	1.299 e-5
Max/min ratio	8.519	16.379
Minimum GLL point distance	1.949 e-5	2.245 e-6
Average GLL point distance	2.822 e-5	3.249 e-6

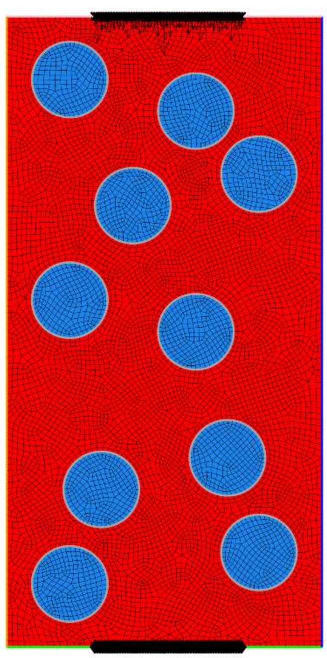

Sample L1

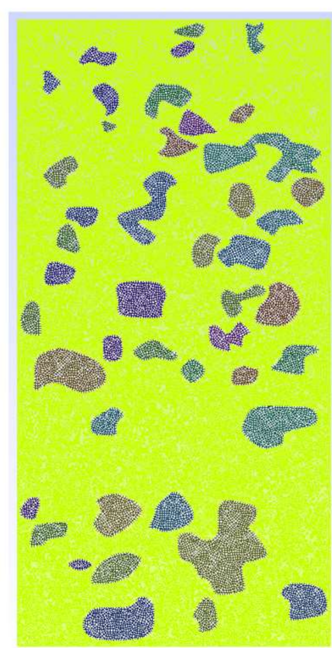

Sample R1H

- Propagation images in displacement for sample L1

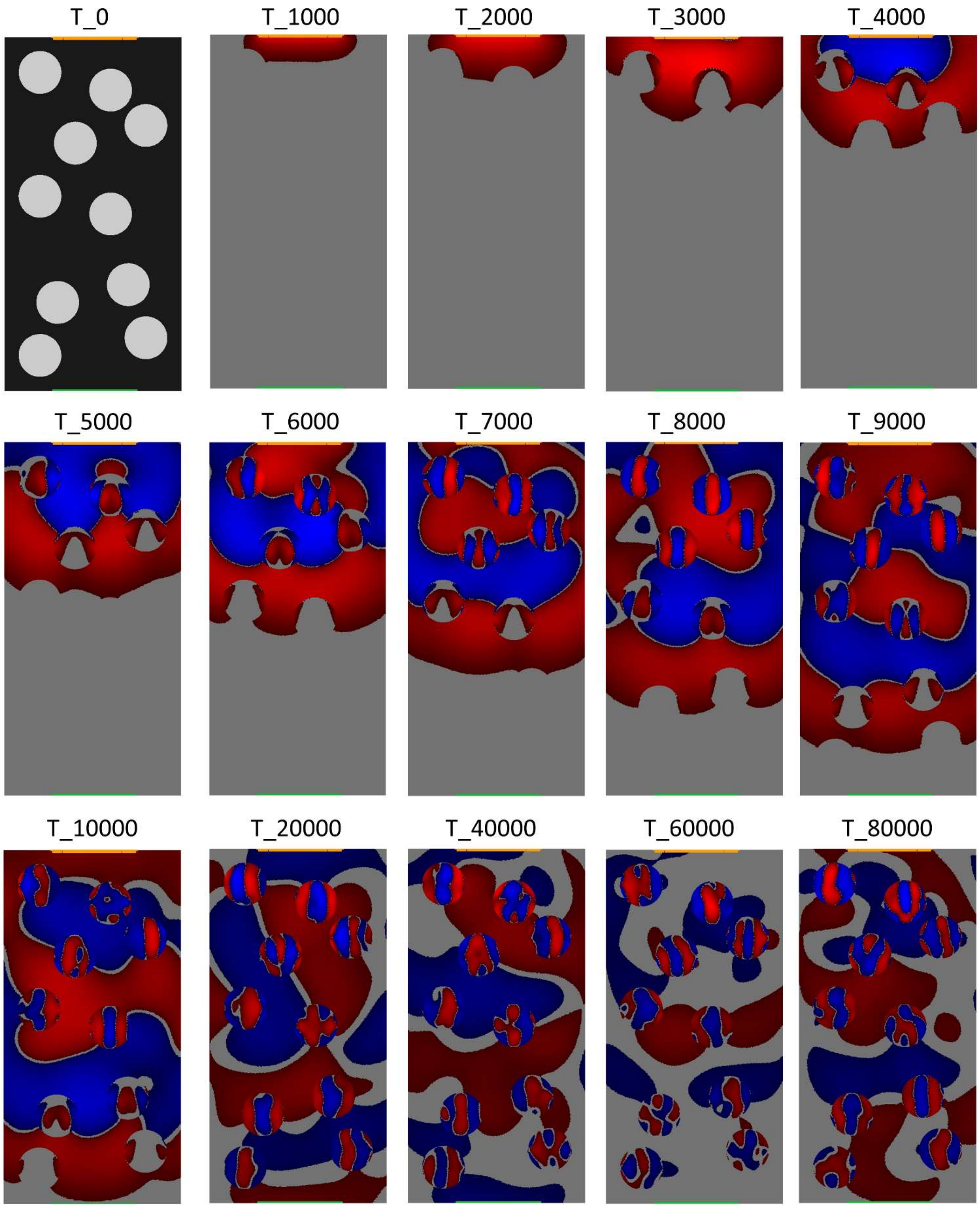

SM-2. Correlation coefficients and Energy ratio.

Table 1. Correlation coefficients for Case-1

	L1	L2	L3	L4	L5
L1	1.00	0.93	0.92	0.92	0.71
L2	0.93	1.00	0.84	0.85	0.49
L3	0.92	0.84	1.00	0.96	0.82
L4	0.92	0.85	0.96	1.00	0.79
L5	0.71	0.49	0.82	0.79	1.00

Negligible (0-0.1)
Weak (0.1-0.39)
Moderate (0.4-0.69)
Stong (0.7-0.89)
Very Strong (0.9-1)

Table 2. Correlation coefficients for Case-2

	p12s1	p6s2	p4s3	p3s4	p2s6
p12s1	1.00	0.68	0.71	0.79	0.73
p6s2	0.68	1.00	0.84	0.82	0.80
p4s3	0.71	0.84	1.00	0.87	0.91
p3s4	0.79	0.82	0.87	1.00	0.88
p2s6	0.73	0.80	0.91	0.88	1.00

Table 3. Correlation coefficients Case-3

	N4	N8	N16	N32	N64
N4	1.00	0.78	0.56	0.48	0.52
N8	0.78	1.00	0.72	0.45	0.54
N16	0.56	0.72	1.00	0.68	0.77
N32	0.48	0.45	0.68	1.00	0.68
N64	0.52	0.54	0.77	0.68	1.00

- Correlations between Cases 1, 2 and 3: **Energy Ratio distribution**.

To better quantify the differences between the three cases we used an attenuation parameter: the energy ratio or the relation between the root-mean-square (RMS) of the wave package and the RMS of the coda. The distribution of energy ratio for Case-3 (Case_number) is the largest; this means that there are significant differences in the waveform between the wave package and the coda when using samples with different amounts of pores, sizes and locations. The range is smallest for Case-1 (Case_loc), in which the geometry and number of pores are constant, and the only variable is the location of the pores in the grid. The range of Case-1 confirms that despite the good correlation estimated between the waveforms of samples L1, L2, L3, L4, and L5, the location of the pores creates indeed a shift in time, amplitudes and phases. Even at these scales and frequencies waveforms and scales are different depending on the propagation path between source and receiver.

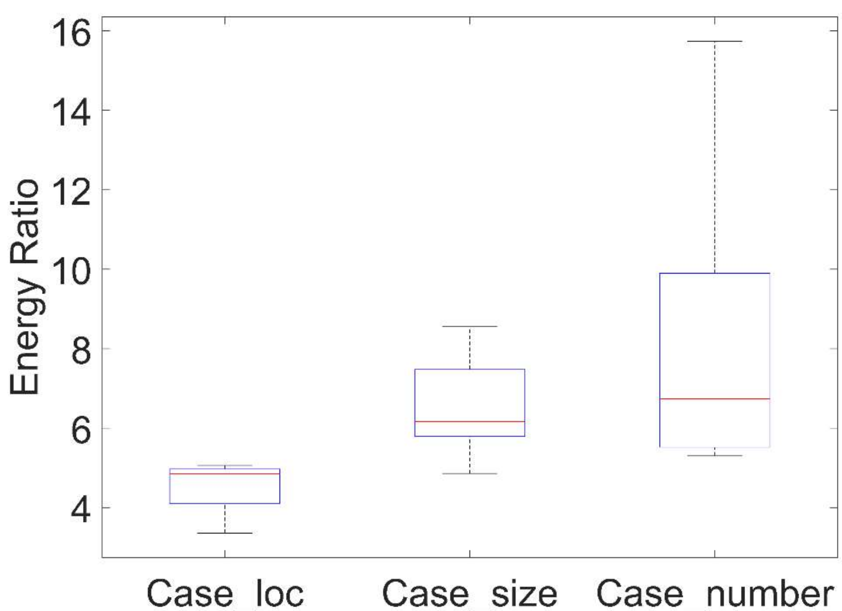

SM-3. Case-C Testing near-field influence on the sensors.

Here we present simulations representative of Case-1 (assessing the role of the location of the pores). However, we decided to design samples in which the pores were located at least λ/2 away from the sensors, to discard the effect of the vicinity of the pores to the receiver and source. The correlation coefficients for Case-C shows a very strong agreement between the waveforms (Table 4). The observations are the same for both scenarios: In samples of the same porosity, with the same number of pores, of the same size and geometry, but in different locations, the correlation between the waveforms is strong. Therefore, when the other parameters are constant, the location of the pores has the lowest impact on the S-wave propagation.

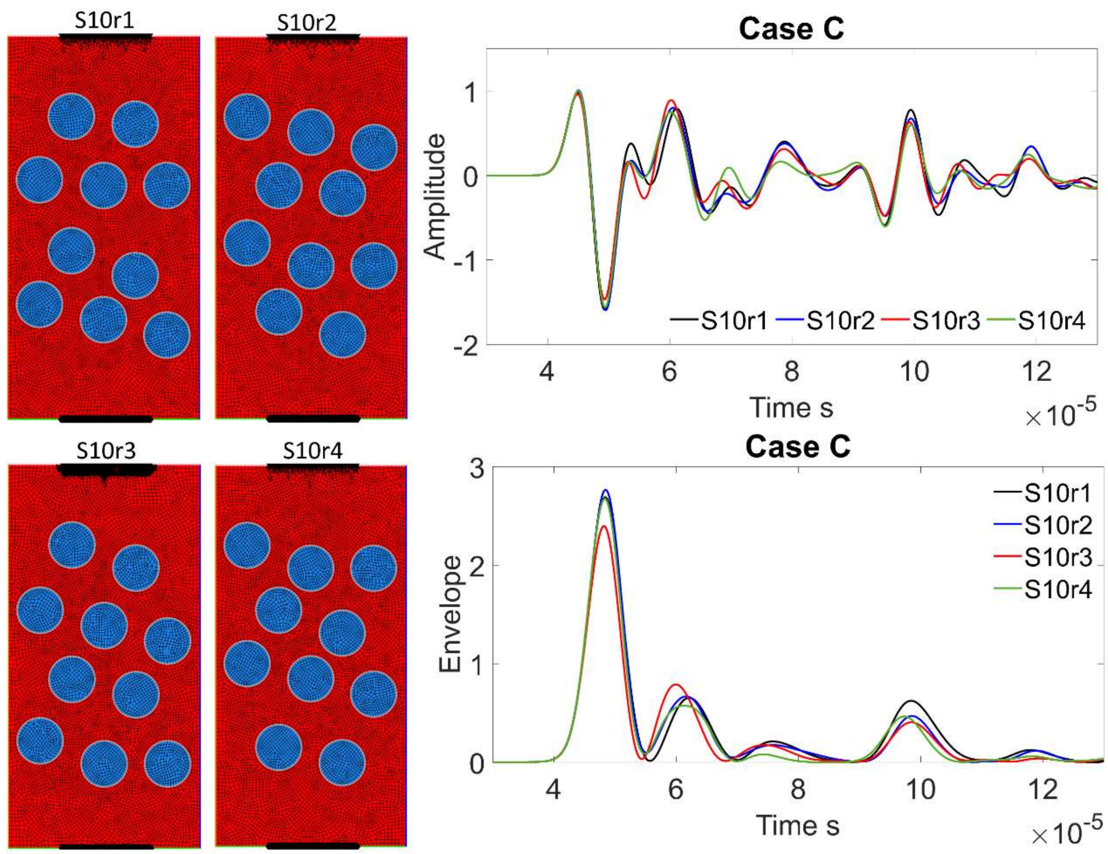

Case-C. Similar to Figure 1 for Case-1. Here the location of the pores between samples was changed systematically and kept at least 1/2λ from source and receiver to remove their near-field influence on the sensors.

Table 4- Correlation coefficient Case -C

	S10	S10r1	S10r2	S10r3
S10	1	0.9731	0.9497	0.9423
S10r1	0.9731	1	0.9649	0.9552
S10r2	0.9497	0.9649	1	0.9523
S10r3	0.9423	0.9552	0.9523	1

SM-4 Creation of synthetic sample S45p

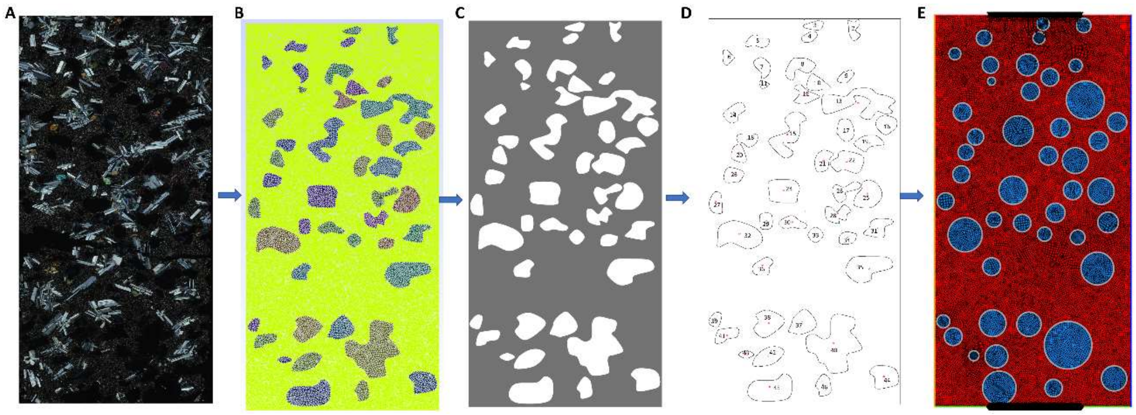

We used a light microscope image of sample 1H (from Di Martino et al., 2021) (A) to manually create a mesh (in Gmesh) with a representation of the largest 45 pores (B: sample R1H). A segmented image (C) was generated (in ImageJ) and measurements of each pore were computed (D, values in table below). The area fraction was converted to mm^2; then we estimated the ratio of a sphere that occupies that area ($a=\pi R^2$) to be used in the mesh of sample R45p (E). The waveform for R45p was computed using 300,000 time steps with a duration of 1 ns each.

#	area px	perimetr	circ	AR	Round	Solidity	Area %	Area mm^2	Ratio mm E (R45p)
2	3352	281.91	0.53	1.88	0.53	0.81	0.23	2.75	0.94
3	2548	223.24	0.64	2.26	0.44	0.96	0.18	2.09	0.82
4	2344	191.72	0.80	1.80	0.56	0.97	0.16	1.92	0.78
5	3880	283.28	0.61	2.19	0.46	0.86	0.27	3.18	1.01
6	2238	192.45	0.76	1.38	0.72	0.93	0.15	1.84	0.76
7	4253	270.88	0.73	1.58	0.64	0.90	0.29	3.49	1.05
8	7413	411.79	0.55	1.82	0.55	0.83	0.51	6.08	1.39
9	2697	210.84	0.76	1.86	0.54	0.96	0.19	2.21	0.84
10	4958	302.64	0.68	1.54	0.65	0.96	0.34	4.07	1.14
11	1040	130.13	0.77	1.32	0.76	0.95	0.07	0.85	0.52
12	5209	358.13	0.51	1.32	0.76	0.80	0.36	4.27	1.17
13	22730	1046.43	0.26	3.00	0.33	0.66	1.57	18.65	2.44
14	5266	296.58	0.75	1.71	0.58	0.93	0.36	4.32	1.17
15	14374	710.71	0.36	2.34	0.43	0.73	0.99	11.79	1.94
16	5936	291.71	0.88	1.13	0.88	0.98	0.41	4.87	1.25
17	5863	293.32	0.86	1.37	0.73	0.98	0.41	4.81	1.24

18	4149	259.48	0.77	1.66	0.60	0.95	0.29	3.40	1.04
19	5745	335.26	0.64	2.09	0.48	0.89	0.40	4.71	1.22
20	3960	249.62	0.80	1.36	0.73	0.98	0.27	3.25	1.02
21	5435	298.74	0.77	1.58	0.64	0.93	0.38	4.46	1.19
22	10448	426.38	0.72	1.56	0.64	0.92	0.72	8.57	1.65
23	4683	266.21	0.83	1.32	0.76	0.97	0.32	3.84	1.11
24	12577	438.45	0.82	1.30	0.77	0.98	0.87	10.32	1.81
25	10855	409.30	0.81	1.30	0.77	0.96	0.75	8.91	1.68
26	5597	385.06	0.47	2.12	0.47	0.77	0.39	4.59	1.21
27	4470	271.14	0.76	1.69	0.59	0.98	0.31	3.67	1.08
28	5787	375.40	0.52	1.66	0.60	0.80	0.40	4.75	1.23
29	3652	230.13	0.87	1.31	0.76	0.98	0.25	3.00	0.98
30	4835	310.64	0.63	2.26	0.44	0.92	0.33	3.97	1.12
31	6667	373.81	0.60	1.64	0.61	0.86	0.46	5.47	1.32
32	18240	581.63	0.68	1.83	0.55	0.91	1.26	14.96	2.18
33	3169	211.91	0.89	1.00	1.00	0.97	0.22	2.60	0.91
34	3432	227.10	0.84	1.46	0.69	0.98	0.24	2.82	0.95
35	16720	559.10	0.67	1.94	0.52	0.93	1.16	13.72	2.09
36	5020	284.84	0.78	1.45	0.69	0.94	0.35	4.12	1.14
37	9212	378.96	0.81	1.24	0.81	0.97	0.64	7.56	1.55
38	11195	426.70	0.77	1.21	0.82	0.95	0.77	9.18	1.71
39	2669	199.48	0.84	1.38	0.73	0.97	0.18	2.19	0.83
40	35467	941.09	0.50	1.26	0.79	0.79	2.45	29.10	3.04
41	5007	304.31	0.68	2.12	0.47	0.94	0.35	4.11	1.14
42	8198	372.33	0.74	2.00	0.50	0.98	0.57	6.73	1.46
43	1593	167.34	0.72	1.98	0.50	0.96	0.11	1.31	0.64
44	10002	403.36	0.77	1.22	0.82	0.94	0.69	8.21	1.62
45	17533	552.82	0.72	1.98	0.51	0.93	1.21	14.38	2.14
46	4769	275.18	0.79	1.49	0.67	0.95	0.33	3.91	1.12

SM-5. Comparison with theoretical models.

In this section, we compare the dynamic shear modulus (computed from the acquired waveforms) with the effective shear modulus estimated from the Kuster and Toksöz

- Kuster and Toksöz (1974) expressions for the effective shear (μ*) moduli:

$$(\mu_{KT}^{*}-\mu_m)\frac{(\mu_m+\vartheta_m)}{(\mu_{KT}^{*}+\vartheta_m)}=\sum_{i=1}^{N}x_i(\mu_i-\mu_m)Q^{mi}$$

- Coefficients *Q* describe the effect of inclusions '*i*' of spherical shapes in a background medium '*m*'. (Berryman, 1995).

$$Q^{mi}=\frac{\mu_m+\vartheta_m}{\mu_i+\vartheta_m} \qquad \vartheta=\frac{\mu}{6}\frac{(9K+8\mu)}{(K+2\mu)}$$

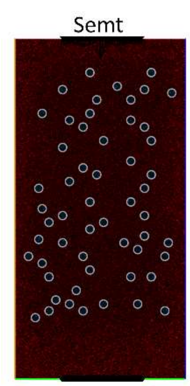

We designed an extra sample (Semt), representative of an effective medium to test the accuracy of the comparisons with the theoretical approximation. This sample has 55 pores of 1.2 mm diameter, which represent 4.97% porosity. The properties for both the matrix and the pores are the same used for the rest of the synthetic samples. Given the small size of the pores, the characteristic length of the elements in the mesh was reduced by 80% and the time step of the simulation was adjusted to 1.0 nanoseconds. Computational limitations restricted us from simulating wave propagation for a sample with 22% porosity that complied with the effective medium theory, this might be assessed in further work.

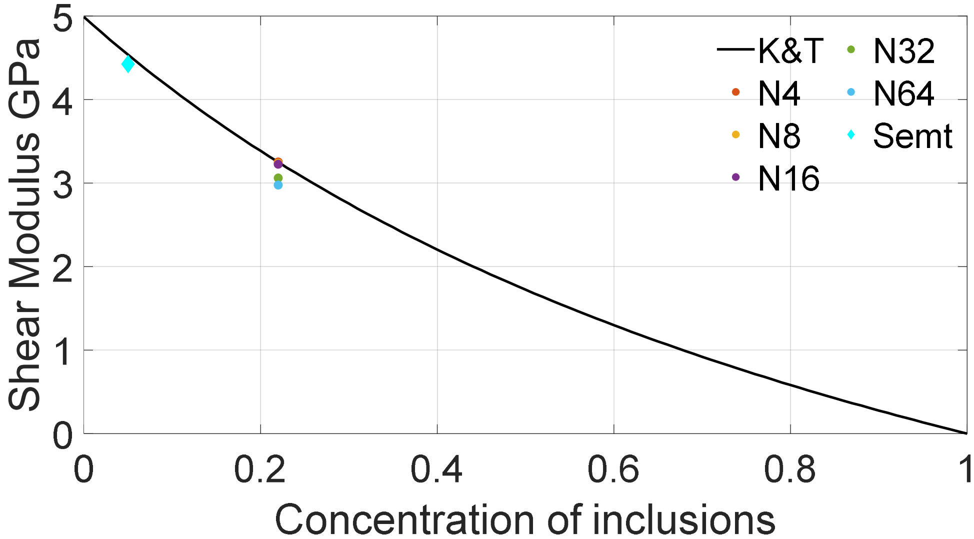

The difference between the theoretical modulus and the one estimated from the simulations for sample Semt is 0.01 GPa for shear modulus (i.e., 0.14% error). While for the synthetic samples the shear modulus diverges between 1.3 and 0.08 GPa with the K&T trend (i.e., 18.8 to 1.15% difference among the samples). These differences are explained by the fact that the samples designed for the simulations done in this study do not comply with the assumptions and limitations of these theories.

SM-6. Absorbing versus reflective boundary conditions.

Absorbing boundary conditions were applied along the physical boundaries of the samples in all the simulations presented in the main manuscript. To observe the effect of reflections and conversions that may occur at the boundaries of the sample, that consequently perturbed the wave propagation, here we show the acquired waveforms for the S-wave propagation in Sample R45p for the case in which the left and right borders of the grid have free boundaries (i.e, reflections at this boundaries are allowed 'R45p-ref').